

# Energy loss and impact cratering in aerogels: theory and experiment

Gerardo Domínguez<sup>a,b,\*</sup>, Andrew J. Westphal<sup>b</sup>, Steven M. Jones<sup>c</sup>, Mark L.F. Phillips<sup>d</sup>

<sup>a</sup> Department of Physics, University of California at Berkeley, Berkeley, CA 94720, USA

<sup>b</sup> Space Sciences Laboratory, University of California at Berkeley, Berkeley, CA 94720, USA

<sup>c</sup> Jet Propulsion Laboratory, California Institute of Technology, 4800 Oak Grove Dr., Pasadena, CA, USA

<sup>d</sup> Pleasanton Ridge Research Corporation, Hayward, CA 94542, USA

Received 8 January 2004; revised 4 June 2004

Available online 25 September 2004

## Abstract

Aerogel collectors have been deployed in low-Earth orbit to collect orbital debris and micrometeorites. An array of silica aerogel collectors is currently en-route back to Earth following an encounter with the Comet Wild-2 on board the Stardust spacecraft. Stardust is returning, for laboratory analysis, cometary and interstellar dust grains which impacted into the aerogel collectors at hypervelocities. While the morphology of impact craters in aerogels has been studied empirically, a theoretical understanding of the physical mechanisms responsible for the formation of impact craters in these solids is lacking. Here we propose and test a model of compaction driven impact cratering in aerogels. Our model derives impact crater dimensions directly from energy and momentum deposition.

© 2004 Elsevier Inc. All rights reserved.

**Keywords:** Cratering; Impact processes; Comets; Asteroids

## 1. Introduction

Silica aerogels are highly porous solids consisting of a network of SiO<sub>2</sub> nanoparticles ( $r_p \sim 10\text{--}100$  nm). They are the lowest density solids known and are commonly prepared via the supercritical solvent extraction of a sol–gel (Gesser and Goswami, 1989). In addition to their unusual physical properties (e.g., low density and thermal conductivity), they have been shown to be superior at capturing hypervelocity ( $v \gg$  speed of sound) projectiles in excess of  $7 \text{ km s}^{-1}$  at least partially intact (Barrett et al., 1992; Kitazawa et al., 1999). This capture process typically results in the formation of a “carrot” shaped impact crater, commonly referred to as a track (see Fig. 1).

NASA’s Stardust mission is currently en route back to Earth following an encounter with the Comet Wild-2 in January 2004. Stardust has collected cometary and interstellar dust grains in SiO<sub>2</sub> aerogel collectors for return

to Earth (Brownlee et al., 1997). Since the early 1990s, several aerogel collectors have been flown in Low-Earth-Orbit (LEO) (e.g., ODCE, EuReCa) (Hörz et al., 2000; Burchell et al., 1999) in part to characterize the orbital debris environment but also with the goal of capturing extraterrestrial particles. These collectors, in addition to recording carrot-shaped tracks, have recorded anomalous track morphologies that appear to have no laboratory analog (Hörz et al., 2000). While some of these are suspected of having originated from extremely fast (and presumably extraterrestrial) micron sized dust grains, to date only a few extraterrestrial projectiles have been identified and analyzed in aerogel collectors deployed in LEO (Hörz et al., 2000; Burchell et al., 1999). Even simple estimates of the kinematic properties of these impact events has been elusive, in large part because the impact cratering process in aerogels is not well understood.

In this paper we propose and test a quantitative model of compaction driven impact cratering in porous solids. While this work is primarily motivated by our desire to understand how aerogel based impact energy detectors work

\* Corresponding author.

E-mail address: [domi@socrates.berkeley.edu](mailto:domi@socrates.berkeley.edu) (G. Domínguez).



Fig. 1. Carrot shaped track found in aerogel exposed on the Mir Space Station. The projectile entered the aerogel from the lower right and is found at the upper left hand corner of the image.

(Domínguez et al., 2003), a theoretical understanding of impact cratering in aerogels could have wider implications.

## 2. Previous work on impacts into aerogel

Previous work on impacts into aerogel largely consist of studies that focus on the effects of the capture process on the projectile. In this section, we provide an historical overview of this work, with an emphasis placed on observations that are relevant to the theoretical model we present.

Early work demonstrated the feasibility of using aerogels to capture hypervelocity projectiles relatively intact (Tsou, 1990; Barrett et al., 1992). Barrett et al. (1992) and Burchell et al. (1999, 2001) have done empirical studies on the scaling of impact cavity dimensions with projectile properties (velocity, projectile density, size) in aerogels of various densities. In addition to examining the effects that the capture process has on 105–125  $\mu\text{m}$  irregularly sized projectiles that consisted of single crystal grains of calcite, olivine, enstatite and pyrrhotite, Barrett et al. (1992) concluded that the track length is not a sensitive function of the velocity but is a strong function of the aerogel density.

Kitazawa et al. (1999) presented empirical data on the track length, mouth diameter, and maximum track diameter. They also estimated projectile ablation in their studies. Their images of tracks from impacts with velocities as high as 12  $\text{km s}^{-1}$  bear some resemblance to the impact cavities found in the ODCE collector that are suspected of being caused by extremely fast impact events. However, the authors' choice of irregular, non-spherical projectiles may have contributed to the large dispersions (more than 2 orders of magnitude in some cases) in their data, since the random effects of projectile tumbling cannot be known. The authors describe the energetics of the capture process using simple drag and ablation models to account for the reduction in size of their captured projectiles and the reduced track length at higher velocities.

Burchell et al. (1999) systematically examined the effects of projectile size and density on the track length and track mouth diameter in  $92(\pm 0.5) \text{ mg cm}^{-3}$  by shooting ( $v = 5.1 \pm 0.2 \text{ km s}^{-1}$ ) a combination of irregularly-shaped olivine (75–375  $\mu\text{m}$ ) and iron projectiles (75–375  $\mu\text{m}$  in diameter) as well as spherical glass beads (75–375  $\mu\text{m}$  in diameter). The scatter in their individual points is large, making it difficult to obtain quantitative information that is sufficiently accurate for our purposes. There are, however, two trends in their data worth mentioning: larger projectiles lead to larger track mouths and longer tracks and denser projectiles lead to longer tracks (Burchell et al., 1999).

Hörz et al. (2000) noted that the length of impact craters in the ODCE aerogel collectors did not systematically correlate with the size of the projectile at the end. This observation has frustrated efforts at reconstructing the original velocity and possible origins of projectiles captured in this collector.

Burchell et al. (2001) fired 106.2  $\mu\text{m}$  ( $\pm 2\%$ ) glass beads into aerogels with various densities ( $\rho = 60, 96, \text{ and } 180 \text{ mg cm}^{-3}$ ) at several velocities (1–7.5  $\text{km s}^{-1}$ ) and reported on the velocity dependence of track length, track volume and track diameter near the surface. Their data, in agreement with Barrett et al. (1992), indicate that the track length does not increase indefinitely as a function of velocity, leading to non-significant correlation between track length and velocity. The track lengths of Burchell et al. (2001) appear to reach a peak, which depends on the density of the target aerogel, although the scatter in the data does not allow one to draw a definite conclusion. Finally, the authors measured the diameters of the captured projectiles and compared them to their original sizes; the size of projectiles captured at the highest velocities may be systematically smaller than the original sizes, especially for the projectiles captured in the 60  $\text{mg cm}^{-3}$  aerogels, but the ambiguity in the data indicate that ablation of the projectiles is not significant at these impact velocities. The authors of these empirical studies did not relate their data to theory.

Theoretical work by Anderson and Ahrens (1994) on the physics of dust grain capture in organic foams focused solely on the energy loss of projectiles and neglects any treatment of the physical mechanisms responsible for the creation of an impact cavity in low density solids. A subsequent report for NASA on the physics of interplanetary dust collection in support of the Stardust mission by Anderson (1998) once again focused only on the stopping of the projectile. A vaporization model for impact cratering in low density foams was proposed by Kadono (1999). We briefly discuss the applicability of this model in Section 4.

## 3. Impact cratering in solids and in aerogels

When a hypervelocity projectile ( $v \gg$  speed of sound) impacts the surface of a target, both the surface and the projectile experience a shock pressure,  $P_{\text{shock}}$  given approx-

imately by

$$P_{\text{shock}} \sim \rho_t v_i^2, \quad (1)$$

where  $\rho_t$  is the density of the target and  $v_i$  is the velocity of the impactor. A shock wave is sent into both the target and the projectile. Upon reaching the rear of the projectile in a time  $t \sim D/U_s$ , where  $U_s$  is the shock wave velocity in the projectile material, a rarefaction wave of comparable strength propagates back from the rear of the projectile and the projectile decompresses. For impacts into ordinary solids ( $\rho_t \sim 3000 \text{ mg cm}^{-3}$ ), the strength of the impact typically results in the complete (or almost complete) destruction of the projectile at or near the surface. A hemispherical shock wave travels into the target that compresses, crushes, deforms and excavates the target material in the vicinity of the impact. These processes result in the formation of an impact crater that is roughly hemispherical in shape. This type of impact event has been well studied because of its applications for cratering on Earth, the Moon, and other Solar System bodies (Melosh, 1989; dePater and Lissauer, 2001).

Hypervelocity impacts into aerogel differ significantly from those into ordinary solids. The tremendous mismatch between the target and projectile densities ( $\rho_{\text{projectile}}/\rho_{\text{target}} \sim 1$  vs.  $\rho_{\text{projectile}}/\rho_{\text{target}} \sim 100/1$ ) allows the projectile to penetrate deeply into the aerogel. As the projectile penetrates and slows, the energy and momentum loss of the impacting hypervelocity projectile is transferred to the aerogel, creating a shock wave that propagates nearly radially away from the projectile's trajectory. Because of the low density (porosity  $\simeq 99\%$ ) and crushing strength of aerogel, this outgoing shock wave compacts the aerogel as it expands and weakens until it can no longer overcome the crushing strength of the aerogel. The relationship between the kinematic properties of the projectile and the final impact cavity morphology is the focus of this paper.

To be quantitative, we consider the energy and momentum loss of the projectile. For simplicity we consider a normally incident spherical projectile of radius  $r_g$  in aerogel. For the discussion that follows, we define a cylindrical coordinate system whose origin is the point of entry into the aerogel and whose  $\hat{z}$  direction coincides with the direction of the projectile. The radial direction ( $\hat{r}$ ) is perpendicular to this direction, pointing away from the trajectory of the projectile.

Trucano and Grady (1995) have shown that the slowing of spherical projectiles captured in ideal porous media (hydrocarbon foams) is adequately described by a hydrodynamic force of the form:

$$F_h = \frac{1}{2} \left( \frac{1+k}{2} \right) \rho_0 v^2 A, \quad (2)$$

where  $A = \pi r_g^2$  and  $k$  is the compressibility of the porous target. We assume that aerogels are ideal porous solids consisting of a low ( $\rho_0$ ) and high ( $\rho_1$ ) density state and com-

pressibility  $k = 1 - (\rho_0/\rho_1) = 1$  (see Zel'dovich and Yu (1967); Trucano and Grady (1995) for more details).

The force exerted by the aerogel resisting compression is given by:

$$F_c = P_c A, \quad (3)$$

where  $P_c$  is the crushing pressure of the aerogel. For later convenience, we can express  $P_c$  as:

$$P_c = \frac{1}{2} \rho_0 v_c^2, \quad (4)$$

where  $v_c$  is the critical velocity for crushing.

The momentum loss of the projectile is given by:

$$\frac{dp}{dz} = -\frac{1}{v} (F_h + F_c) = -\frac{C_d}{2} \rho_0 v_g^2 A - P_c A, \quad (5)$$

where  $\rho_0$  is the uncompressed density of the aerogel,  $v_g$  is the instantaneous velocity,  $A$  is the cross sectional area of the projectile. In general we expect  $C_d \simeq 1$ , but we will treat it as a parameter to quantitatively describe any additional slowing. Assuming  $r_g$  is constant, Eq. (5) can be solved to give:

$$v_g(z) = v_0 e^{-z/(2\lambda)} \left[ 1 + \frac{1}{C_d} \left( \frac{v_c}{v_0} \right)^2 (1 - e^{z/\lambda}) \right]^{1/2}, \quad (6)$$

where  $\lambda$  is given by:

$$\lambda = \frac{1}{C_d} \frac{4}{3} \frac{\rho_g}{\rho_0} r_g. \quad (7)$$

For  $v > 0.5 \text{ km s}^{-1}$ , the crushing term can be neglected and the kinetic energy of the projectile becomes:

$$E(z) \simeq E_0 e^{-z/\lambda}, \quad (8)$$

where  $E_0 = \frac{1}{2} m_g v_0^2$  is the initial kinetic energy of the projectile and  $m_g = \frac{4}{3} \pi \rho_g r_g^3$ .

The energy and momentum lost by the projectile per unit length is transferred to the aerogel material that it encounters. Employing momentum conservation, we find that the velocity of the shocked aerogel along the  $\hat{z}$  direction is given by:

$$v_{s,z}(r = r_g, z) = C_d \frac{v_g(z)}{2}. \quad (9)$$

The acceleration of the uncompressed aerogel by the shock is analogous to an inelastic collision. While momentum is conserved in the collision, the kinetic energy is not. The energy transfer to the newly shocked material is split equally into kinetic and thermal energy components (see Appendix A for more details). We can express this condition as:

$$\frac{1}{2} \rho_0 \pi r_g^2 (v_{s,r}^2 + v_{s,z}^2) = \frac{1}{2} \frac{dE}{dz}. \quad (10)$$

Here  $v_{s,z} = \vec{v}_s \cdot \hat{z}$ ,  $v_{s,r} = \vec{v}_s \cdot \hat{r}$ , and  $\vec{v}_s$  is the velocity vector of the shocked aerogel.

Using Eqs. (9) and (10), one can show that the radial component of the shocked aerogel immediately after the passage

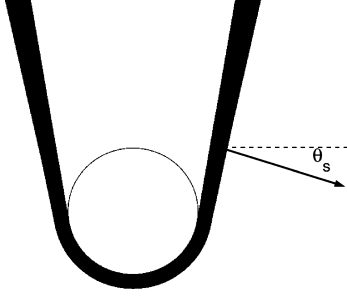


Fig. 2. Shock wave propagation into aerogel at points away from the surface.  $\theta_s = 45^\circ$  when  $C_d = 1$ .

of the projectile is given by:

$$v_{s,r}(r = r_g, z) = v_g(z) \left( \frac{C_d}{2} - \frac{C_d^2}{4} \right)^{1/2}. \quad (11)$$

Far from the surface, Eqs. (9) and (11) imply the shock wave travels at an angle  $\theta_s$  with respect to the radial direction axis, independent of velocity (and hence location along the trajectory). This angle is given by:

$$\tan \theta_s = \frac{C_d}{2 \left( \frac{C_d}{2} - \frac{C_d^2}{4} \right)^{1/2}}. \quad (12)$$

This result is illustrated by Fig. 2. Note that in the case of a blunt object,  $C_d = 2$  and in this case all of the momentum and kinetic energy are transferred only in the  $\hat{z}$  direction.

We are interested in the kinetic component of the shock wave. Using (A.2) and Eqs. (9) and (11), we find that the kinetic pressure of the shock wave at the interface between the projectile and the aerogel is given by:

$$P_k(r = r_g, z) = \frac{C_d}{2} \rho_o v_g^2(z). \quad (13)$$

The attenuation of a compaction shock wave in ideal porous media, regardless of geometry, can be shown to scale as:

$$P \propto M^{-2}, \quad (14)$$

where  $M$  is the mass of the compressed shock front. For clarity, we have included an outline of a derivation, similar to that found by Zel'dovich and Yu (1967), in Appendix B.

Because the shock wave angle is independent of velocity, we conclude, assuming that the shock wave is cylindrical and using Eq. (B.21), that the ram pressure of the cylindrical shock wave of compressed aerogel away from the surface region is given by:

$$P_k(r, z) = \frac{C_d \rho_o}{2} v_g^2(z') \left( \frac{r_g \cos \theta_s}{r} \right)^4, \quad (15)$$

where  $z' = z - r_T \tan \theta_s$  and  $r(z)_T$  is the radius of track. Note that  $P_s(r = r_g, z)$  is consistent with Eq. (13). In addition, because  $\theta_s$  is not zero, the final size of the impact crater at a given  $z$  is determined by the energy and momentum deposition upstream. This in part explains why the largest opening of an impact cavity in aerogels is not found at the surface of the aerogel. The strength of the shock wave at and near

the surface is strongly attenuated ( $P_k(r) \propto r^{-6}$ ) because the geometry of the expansion in this region is spherical. We conclude that the general shape of impact cavities in aerogels is determined by the expansion of a spherical shock at and near the surface followed by a gradual transition into a domain of cylindrical expansion. The transition between spherical and cylindrical geometry occurs within a region given approximately by  $\Delta z \sim r_T(0) \tan \theta_s$ . A quantitative description of this transition region is beyond the scope of this paper.

For the purpose of comparing the predictions of this model with experimental impact craters, we will ignore the surface and transition regions. In addition, we will approximate  $v(z') \rightarrow v(z)$ . Given the exponential form of  $v(z)$  (see Eq. (6)) and the fact that track radii are typically only a few times the size of the projectile, the error introduced by this approximation is negligible.

The shock wave ceases to expand into the aerogel when  $P_k$  is equal to the crushing strength of the aerogel (or equivalently, when  $|\vec{v}_s| = v_c$ ). Thus, the track radius away from the surface and transition region is given by:

$$r_T(z) = r_g \cos \theta_s \left( \frac{C_d \rho_o v(z)^2}{2 P_c} \right)^{1/4}. \quad (16)$$

## 4. Results

Between December 2001 and October 2003 we exposed samples of silica aerogel of various densities to hypervelocity glass beads at various velocities using the NASA Ames Vertical Gun Range (AVGR). We imaged impact craters in the samples and calibrated them using a microscope and an optically encoded computer-controlled stage.

Various projectiles were used in these shots, including a population of monodisperse glass beads  $20.3 \pm 1.4 \mu\text{m}$  in diameter and a dispersion in size of 9.4%. Because of their relatively tight dispersion most of the analysis that we present here will focus on tracks created by the 20- $\mu\text{m}$  glass beads.

### 4.1. Determining $P_c$

We determined the crushing strength of aerogels empirically by exposing samples with  $\rho = 14, 20, 30, 60, 100 \text{ mg cm}^{-3}$  (prepared by S.M.J.) to mono-disperse 20- $\mu\text{m}$  glass beads at  $4.36 \text{ km s}^{-1}$  during October of 2003. The size of the maximum impact radius, observable near the surface, together with Eq. (16) allowed us to determine  $P_c(\rho)$  with reasonable precision.

Assuming  $C_d = 1$ , we can solve Eq. (16) for  $P_c$  to give:

$$P_c(\rho_o) = \left( \frac{1}{8} \right) \rho_o v_o^2 \left( \frac{r_g}{R_m} \right)^4, \quad (17)$$

where  $R_m = r_T(0)$  and  $\theta_s = 45^\circ$ .

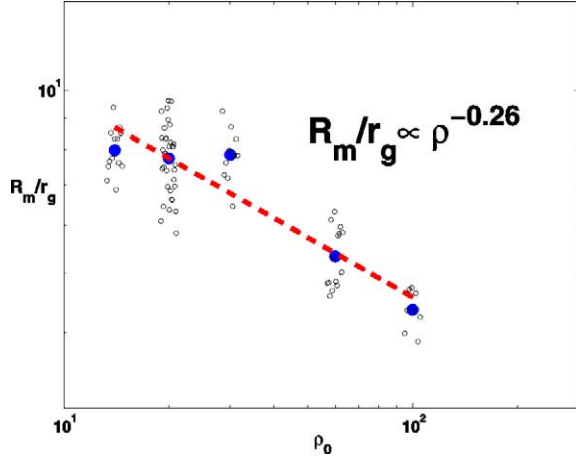


Fig. 3. Individual data points are shown as black dots. Blue dots indicate statistical averages. Dashed red line indicates fit to data, given by  $R_m/r_g \simeq 8.7 \left( \frac{\rho_0}{14 \text{ mg cm}^{-3}} \right)^{-0.26}$ .

We display the individual measurements of the normalized maximum impact radius in Fig. 3 versus aerogel density. We observe that the dispersion in the data for the aerogels of 14, 20, 30, 60, and 100  $\text{mg cm}^{-3}$  were 14, 20, 16, and 18%, respectively, and indicate that, in addition to the dispersion in projectile size, there are other sources of error, possibly due to a dispersion in impact velocities.

Previous work has found that, for a given preparation technique, the mechanical properties of aerogels (Young's Modulus, sound speed, etc.) are power-law functions of their density (Moner-Girona et al., 1999). We similarly assume that  $R_m(\rho_0)$  is a power law and find that it scales as  $R_m/r_g \simeq 8.7 \left( \frac{\rho_0}{14 \text{ mg cm}^{-3}} \right)^{-0.26}$  (see Fig. 3). This result, together with Eq. (17), implies that the crushing strength of the silica aerogels used in our studies scales as:

$$P_c(\rho) \simeq 6 \left( \frac{\rho}{14 \text{ mg cm}^{-3}} \right)^{2.04} \text{ kPa.} \quad (18)$$

It is interesting that the crushing strength  $P_c$  of the aerogels studied here agree in scaling and magnitude to the micro-mechanical hardness  $H$  that Moner-Girona et al. (1999) found in their studies. Although the precise relationship between  $P_c$  and  $H$  is not known, their comparison suggests that they are similar measures of aerogel's resistance to being compressed.

#### 4.2. Track lengths and energy loss of projectiles in aerogel

In the absence of projectile ablation or aerogel accretion, Eq. (6) can be solved exactly for the penetration depth  $L_T$ . This is given by:

$$L_T = \lambda \ln \left( 1 + \left( \frac{v_0}{v_c} \right)^2 \right) \quad (19)$$

$$= \frac{4r_g}{3C_d} \left( \frac{\rho_g}{\rho_0} \right) \ln \left( 1 + \left( \frac{v_0}{v_c} \right)^2 \right). \quad (20)$$

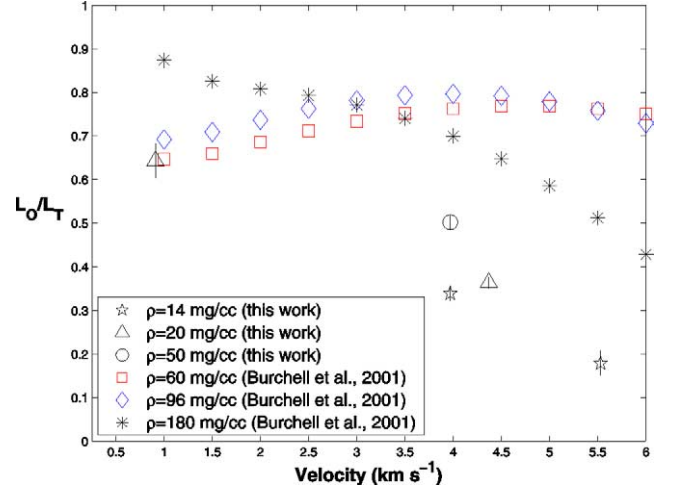


Fig. 4.  $L_O/L_T$  vs. velocity.  $L_O$  is the observed length of impacts in aerogel.  $L_T$  is the expected length of tracks as given by (19) assuming that  $P_c$  is given by Eq. (18).

Thus, the length of tracks in aerogel should scale linearly with projectile size and density, and logarithmically with velocity.

A very good approximation to the above equation is obtained by assuming that  $v_g(z)$  is a simple exponential and requiring that the projectile stop when  $\frac{1}{2}\rho_0 v_g(z = L_T)^2 = P_c$ . The track length in this case is given by:

$$L_T = \lambda \ln \left( \frac{v_0}{v_c} \right)^2. \quad (21)$$

Equations (19) and (21) agree with each other to within 10% or less for  $v_0 > v_c$  and converge with increasing accuracy for higher  $v_0$ .

The actual dynamics of slowing in aerogel are complicated by the ablation, deformation, and (possibly) fragmentation of the projectile. For example, Trucano and Grady found that millimeter sized copper projectiles deformed for high impact velocities ( $v \geq 2.9 \text{ km s}^{-1}$ ) in  $176 \text{ mg cm}^{-3}$  polyurethane foam. The penetration depth of the projectiles is reported to drop by a factor of about 2.5 between  $v = 2.5 \text{ km s}^{-1}$  and  $v = 2.9 \text{ km s}^{-1}$ . This drop in penetration depth (analogous to our  $L_T$ ) is attributed to the permanent plastic deformation of the projectile. For velocities greater than  $4 \text{ km s}^{-1}$ , the authors report that the copper projectiles fragmented, resulting in even shorter penetration depths.

We compare the lengths of tracks from our experiments with theoretical predictions of Eq. (19) in Fig. 4. We have also included the track lengths reported by Burchell et al. (2001) for comparison. An examination of the track lengths (normalized by their theoretical expectation) clearly indicates that the slowing of projectiles is not as straightforward as Eq. (5) suggests. While it is possible that we have underestimated the mechanical strength of the aerogels, this underestimation would have to be severe in order for it to account for our results. Comparison of the track lengths at  $4 \text{ km s}^{-1}$  for the 14 and  $50 \text{ mg cm}^{-3}$  aerogels, in addition,

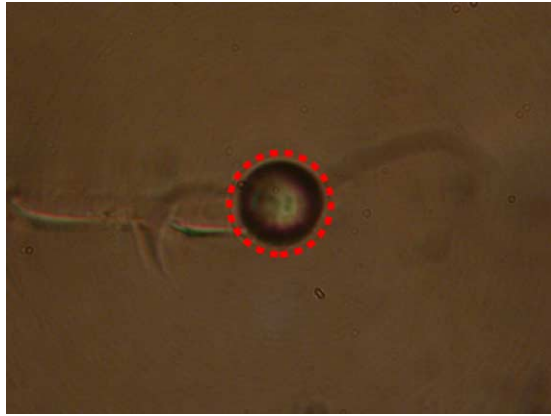
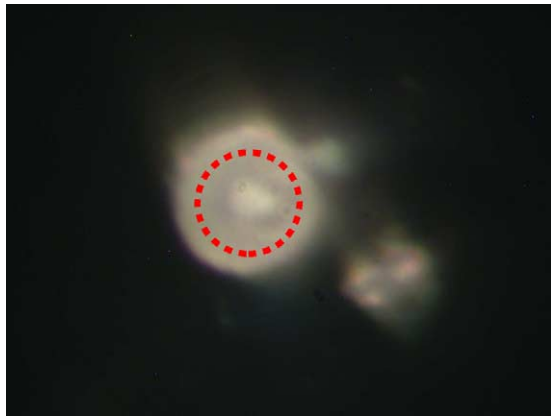
(a)  $\rho = 50 \text{ mg cm}^{-3}$ ,  $v = 1.31 \text{ km s}^{-1}$ .(b)  $\rho = 50 \text{ mg cm}^{-3}$ ,  $v = 3.97 \text{ km s}^{-1}$ .

Fig. 5. Aerogel accretion of 20- $\mu\text{m}$  glass beads captured in 50  $\text{mg cm}^{-3}$  aerogel. A 20- $\mu\text{m}$  circle is overlaid to indicate the probable location of the projectile and scale of the image.

seem to indicate that the track length shortening is density dependent.

Previous studies have attributed track length shortening to projectile ablation (Anderson and Ahrens, 1994; Kitazawa et al., 1999). And, while this possibility cannot be discounted from our data, we suggest another contribution to track length shortening. We observe that, for a given shot, the projectiles at the end of tracks in both the 14, 20, and 50  $\text{mg cm}^{-3}$  aerogels are usually covered in variable amounts of aerogel, especially at higher velocities (Figs. 5 and 6). The dispersion in the track lengths shown in Table 1 at the highest velocities is consistent with this interpretation, although projectile fragmentation may also be a factor at the highest velocities.

Aerogel accretion onto captured projectiles has previously been observed (Barrett et al., 1992; Hörz et al., 2000), although its implications on the length of impact craters has not been treated quantitatively.

For the purposes of our discussion, it is safe to say that the relative contributions of projectile ablation and accretion to the slowing dynamics of projectiles are not well understood. Therefore, our analysis of impact craters in aerogels will focus on the portion near the surface, where the effects

(a)  $\rho = 14 \text{ mg cm}^{-3}$ ,  $v = 3.97 \text{ km s}^{-1}$ .(b)  $\rho = 14 \text{ mg cm}^{-3}$ ,  $v = 5.53 \text{ km s}^{-1}$ .

Fig. 6. Aerogel accretion onto 20- $\mu\text{m}$  glass beads captured in 14  $\text{mg cm}^{-3}$  aerogel. A 20- $\mu\text{m}$  circle is overlaid to indicate the probable location of the projectile and scale of the image.

Table 1

The dispersion in the track length of 20- $\mu\text{m}$  glass beads captured in aerogels of various densities

$D_g$ ( $\mu\text{m}$ )	$\rho$ ( $\text{mg cm}^{-3}$ )	$v$ ( $\text{km s}^{-1}$ )	% dispersion
20	50	1.31	$9 \pm 3$
20	50	3.97	$9 \pm 3$
20	20	0.91	$15 \pm 6$
20	14	3.97	$11 \pm 5$
20	20	4.37	$9 \pm 4$
20	14	5.53	$39 \pm 17$

Note that the dispersion of track lengths at the lower velocities agrees with the dispersion of the projectile size (9.4%), as would be expected for tracklengths dominated by the size of the projectile. The dispersion is especially large for shots with  $v = 5.53 \text{ km s}^{-1}$  into 14  $\text{mg cm}^{-3}$ .

of ablation and accretion should not significantly affect the size and velocity of the projectile.

#### 4.3. Track diameters in 50 $\text{mg cm}^{-3}$ aerogel

Using Eqs. (17) and (16), we independently verified our model by measuring the maximum normalized radius of an impact crater,  $R_m/r_g$ , in samples of 50  $\text{mg cm}^{-3}$  aerogel. Most of our data points were derived from impacts with

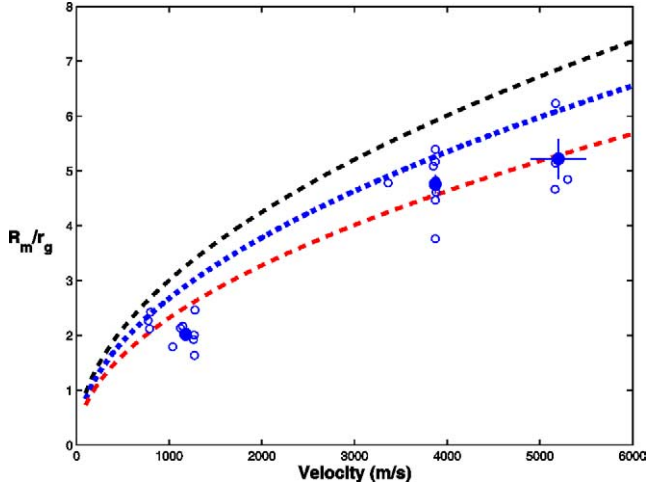


Fig. 7. Velocity scaling of  $R_m/r_g$  for shots into  $50 \text{ mg cm}^{-3}$  aerogels. Blue circles indicate individual data points, while solid blue dots indicate statistical averages. Dashed line (black) indicates prediction of track shape model when  $P_c$  is determined using Eq. (17). A better fit is obtained if  $P_c$  is extrapolated from the experimentally derived value of the  $60 \text{ mg cm}^{-3}$  aerogel assuming a  $P_c \propto \rho_0^2$ . The dashed red line denotes the fit that is obtained if we assume that  $P_c = 17(\frac{\rho}{14 \text{ mg cm}^{-3}})^2$ , the hardness given by Moner-Girona et al. (1999).

20- $\mu\text{m}$  glass beads, although when available, we also included measurements of 2, and 5  $\mu\text{m}$  in diameter glass beads. Figure 7 shows that  $R_m \propto v^{1/2}$  as expected.

To illustrate the ability of our model to mimic the general behavior of track shapes in aerogels, we superimpose model predictions onto images of impacts in  $50 \text{ mg cm}^{-3}$  aerogel at various velocities in Fig. 8.

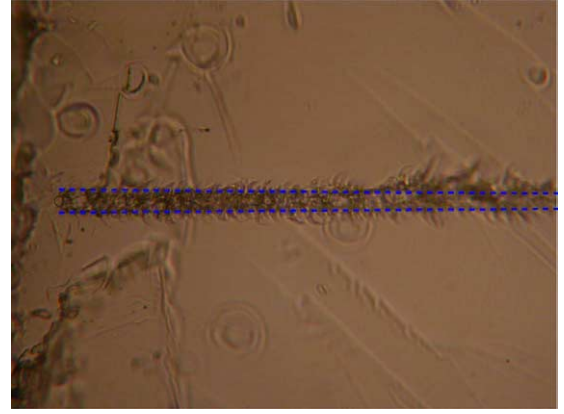
An alternative model of impact cratering in low density solids was proposed previously by Kadono (1999). In his model, he argues that impact craters in porous solids result from the vaporization of the target material. A simple estimate of both the scaling and magnitude of the track radius reveals that vaporization alone cannot suitably account for the dimensions of tracks in silica aerogels. Assuming that all of the projectile energy loss per unit track length ( $\frac{dE}{dz}$ ) is deposited as heat, the radius of vaporized track material resulting from the impact of a projectile with radius  $r_g$  and velocity  $v_g$  is given by:

$$r_{\text{vap}} = r_g \left( \frac{v_g^2}{H_{\text{vap}}} \right)^{1/2} \quad (22)$$

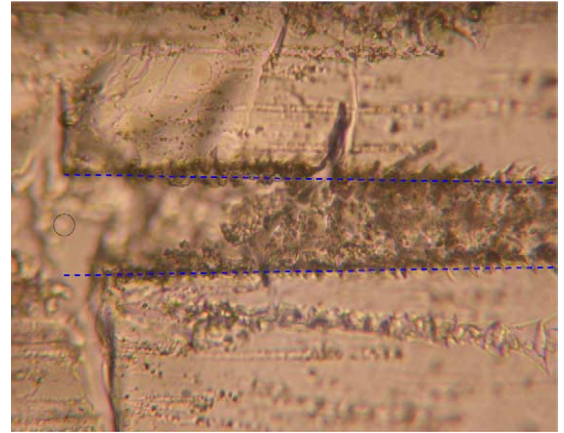
$$\simeq r_g \left( \frac{v_g}{5.6 \text{ km s}^{-1}} \right). \quad (23)$$

Here we assume that  $H_{\text{vap}} = 32.3 \times 10^6 \text{ J kg}^{-1}$ , the standard value for silica. The vaporization model clearly underestimates the size of tracks. The effects of aerogel vaporization may not be negligible at impact velocities exceeding  $5 \text{ km s}^{-1}$  and could complicate the functional dependence of track shapes on projectile properties.

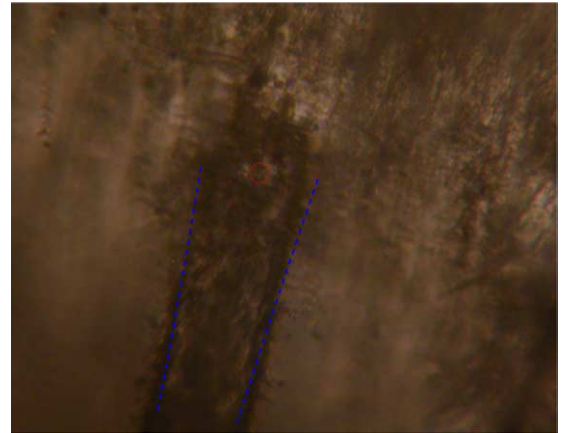
Hörz and others have previously noted that projectiles in aerogel do not necessarily follow straight paths (Hörz et al., 2000). Tracks in our samples also meander, especially at the



(a)  $\rho = 50 \text{ mg cm}^{-3}$ ,  $v = 1.31 \text{ km s}^{-1}$ .



(b)  $\rho = 50 \text{ mg cm}^{-3}$ ,  $v = 3.97 \text{ km s}^{-1}$ .



(c)  $\rho = 50 \text{ mg cm}^{-3}$ ,  $v \simeq 5.3 \text{ km s}^{-1}$ .

Fig. 8. Track shapes near the surface in  $50 \text{ mg cm}^{-3}$  aerogel at various velocities. A circle of 20- $\mu\text{m}$  in diameter has been added to indicate the scale of the projectile and image.

higher velocities in the  $14 \text{ mg cm}^{-3}$  shots. We suggest that this meandering behavior may result from the random and asymmetric accretion and shedding of aerogel during capture, although we cannot rule out projectile spinning.

Because the radius of an impact is a linear function of the projectile radius, the accretion of aerogel can have a drastic effect on track radius. In the absence of aerogel accretion,

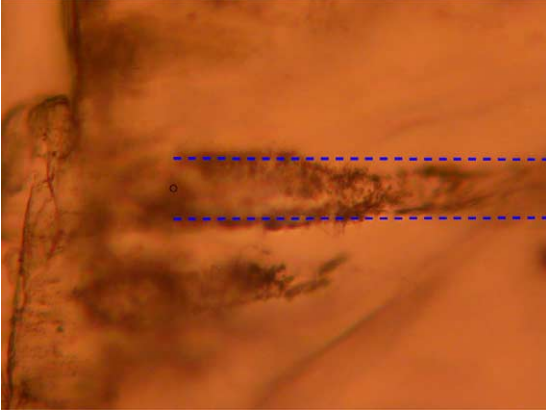


Fig. 9. Irregular track shape profile from the impact of 20- $\mu\text{m}$  glass beads captured in  $14 \text{ mg cm}^{-3}$  aerogel at  $5.53 \text{ km s}^{-1}$ . This track morphology may be indicative of random aerogel accretion and shedding. Note the fluctuations in track radius and apparent wall thickness.

the track radius should be a smooth decreasing function of the distance from the surface in the cylindrical regime. Departures from this behavior indicate that the projectile size is undergoing sudden increases or decreases. For example, Fig. 9 shows a portion of a track shape of an  $5.53 \text{ km s}^{-1}$  impact into  $14 \text{ mg cm}^{-3}$  aerogel that appears to be the result of aerogel accretion and shedding or possibly projectile fragmentation.

#### 4.4. Scaling properties of impact events in aerogel

Our impact cratering model predicts that track dimensions are weak functions of projectile kinematic properties. In summary, the track length scales as:

$$L_T \propto r_g \left( \frac{4\rho_g}{3\rho_0} \right) \ln \left( 1 + \left( \frac{v_0}{v_c(\rho_0)} \right)^2 \right). \quad (24)$$

The track radius away from the surface and transition region scales as:

$$r_T \propto r_g \left( \frac{v}{v_c} \right)^{1/2}. \quad (25)$$

The track volume of an impact crater in aerogel is given by:

$$V_T = \int_0^{L_T} \pi (r_T(z))^2 dz. \quad (26)$$

Away from the surface, the track radius is given by  $r_T(z) \simeq r_g \left( \frac{\rho_0 v^2(z)}{2P_c} \right)^{1/4}$ . If we set  $v_c = 0$ , the volume of the track takes on the analytic form of:

$$V_T \sim \pi r_g^2 \left( \frac{\rho_0 v_0^2}{2P_c} \right)^{1/2} (4\lambda) (1 - e^{-L_T/(4\lambda)}), \quad (27)$$

where  $\lambda = \left( \frac{4}{3} \right) \left( \frac{\rho_g}{\rho_0} \right) r_g$  and  $C_d = 1$ .

Using Eq. (21), the track volume can be expressed as:

$$V_T \sim 4V_p \left( \frac{\rho_g}{\rho_0} \right) \left( \frac{v_0}{v_c} \right) \left( 1 - \left( \frac{v_c}{v_0} \right)^{1/2} \right), \quad (28)$$

where  $V_p = \frac{4}{3} \pi r_g^3$ .

Thus, while the track diameter is expected to be a weak function of the velocity, the volume of the impact cavity is expected to scale linearly with both the volume and velocity of the projectile. In addition, the track volume is not expected to be a straightforward function of the kinetic energy since  $v_c$  is a function of the aerogel density as well.

## 5. Conclusion

We have developed and tested a theoretical model of impact cratering in aerogels. In the case of track diameters near the surface, the correspondence between experiment and theory is good and indicates that the physics of impact crater formation in aerogels is well described by a model in which an outgoing cylindrical shock wave attenuates, in a manner analogous to that of a supernova in the interstellar medium during the momentum conserving “snowplow” phase, and stops when it is no longer able to overcome the mechanical strength of the aerogel.

The correspondence between experimental and theoretical track lengths, on the other hand, is not as satisfactory. The dynamics of projectile slowing are clearly complicated by a variety of factors, including projectile ablation and aerogel accretion. Aerogel accretion onto captured projectiles has been reported by other authors, although to our knowledge the connection between it and the slowing of projectiles has not been pointed out previously. Given the amount of aerogel accretion that we observe, we conclude that its effect on the slowing of projectiles in low density aerogels with micron-sized projectiles is significant. Some amounts of aerogel accretion were observed in the studies of M. Burchell, although this was not observed to be significant (personal communication). We speculate that the enhancement we observe may be due to the higher temperatures that aerogels of lower density experience. To illustrate, we consider the third Rankine–Hugoniot equation. For a given velocity and common final density ( $1/\rho_1$ ), the compression of aerogel from a density  $\rho_0$  to a density  $\rho_1$  changes the internal energy by:

$$E - E_0 = (P + P_0)(V_0 - V)/2, \quad (29)$$

where  $V_0 = 1/\rho_0$  and  $V = 1/\rho_1$  (dePater and Lissauer, 2001). This equation implies that the change in internal energy is inversely proportional to the initial density. Thus, for a given impact velocity, shock compressed ultra-low density aerogels (e.g., 14 and  $50 \text{ mg cm}^{-3}$ ) are expected to be hotter compared to aerogels with higher initial densities. In the design of aerogel collectors, a premium is placed on making aerogels of low-density to reduce the heating rate as well as the impact shock pressure. The observations we make here, however, imply that low density aerogel collectors may actually heat a captured projectile more than would otherwise be expected, due to the

coating of hot aerogel that they accumulate. To what extent the similar composition of the aerogel and glass beads may enhance aerogel accretion should be studied in the future using monodisperse projectiles that are similar in size but different than aerogels in composition. In addition, empirical studies of the viscosity of shocked aerogel could turn out to be helpful in bridging the gap between experimental observation and theoretical predictions of track lengths.

Our model of impact cratering in aerogels predicts that the dimensions of an impact into aerogel are very weak functions of the projectile properties. Efforts to correlate the radius and projectile kinetic energy have not revealed the functional dependences that we predict because these dependences are very weak. It is not surprising that Burchell et al. (1999) observed that projectiles of different density, but same size, produced track radii that were virtually identical. On the other hand, the scaling of the track volume ( $V_T \propto r_g^3 (\frac{\rho_g}{\rho_0}) v_0$ ) does depend on the projectile composition and on the velocity. Of course, natural projectiles are not spherical and will ablate, fracture and even completely disintegrate as a result of the capture process, complicating the reconstruction of the original impact velocity.

Studies of the relationship between energy deposition and track shapes for various projectile types may be augmented with the use of calorimetric aerogels (Domínguez et al., 2003). These aerogel collector/detectors offer the ability to accurately reconstruct the kinetic energy of an impact by using the *total* amount of kinetic energy transferred to the aerogel, in the form of heat and resultant fluorescent material, as an indicator of projectile kinetic energy. This technique, combined with an independent measure of the projectile mass (both at the end of the track and along the impact cavity wall surface), should allow for the accurate reconstruction of projectile kinetic energy. The theoretical model presented here will be used in our efforts to understand the response of these detectors/collectors of hypervelocity impacts.

Finally, the general theoretical method presented here could have applications for studying compaction driven impact cratering in porous Solar System bodies such as comets and asteroids (Kadono, 1999; Housen and Holsapple, 2003; Housen et al., 1999).

## Acknowledgments

We thank Don Bowling, Chuck Cornelison, Don Holt, Rick Smyth, and Pete Schultz for making these shots possible. In addition, many thanks are owed to Christopher Snead for his advice on the preparation of impact samples. Finally, G. Domínguez acknowledge the National Physical Science Consortium Fellowship and Corning Inc. for their financial support.

## Appendix A. Derivation of Rankine–Hugoniot equations

The Rankine–Hugoniot equations express the relationship between the macroscopic properties (density, particle velocity, and energy density) on either side of a shock wave. In the discussion that follows, see Fig. A.1 for the meaning of the various quantities.

Conservation of mass across the interface gives:

$$\rho_0 U_s = \rho_1 (U_s - u_1), \quad (\text{A.1})$$

where  $u_1$  is the particle velocity in the shocked portion of the material.

Conservation of momentum and together with (A.1) yields the second Hugoniot relation:

$$\rho_0 U_s u_1 = P_1 - P_0. \quad (\text{A.2})$$

Similarly, energy conservation and Eqs. (A.1) and (A.2) imply that:

$$E_1 - E_0 = \frac{1}{2} \rho_0 u_1^2. \quad (\text{A.3})$$

Here  $E_1$  and  $E_0$  represent the internal energy (not including enthalpy) of the fluid on either side of the shock. The total amount of work done ( $\rho_0 u_1^2$ ) on the newly shocked fluid together with Eq. (A.3) demonstrates that during the shock compression of materials, half the energy goes into the internal energy and the other half goes into kinetic energy, regardless of the type of material being shocked. In the absence of phase transformations, the internal energy is exactly equal to the heat content of the material.

## Appendix B. Spherical and cylindrical shock wave attenuation in ideal porous media

The authors of (Zel'dovich and Yu, 1967) proposed a simple model for treating shock wave propagation in ideal porous media. In this next section, we reproduce some of their arguments and results.

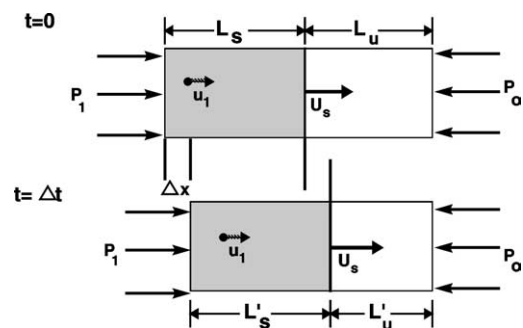


Fig. A.1. The boundary between shocked and unshocked material.  $U_s$  is the shock front velocity.

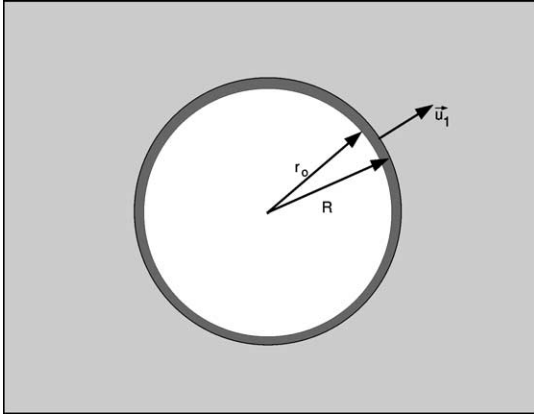


Fig. B.1. Shock wave expansion in porous medium with radial symmetry. Dark gray area is compressed material and light gray represents uncompressed material.

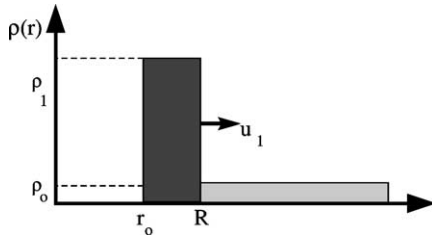


Fig. B.2. Density profile of a shock wave with radial symmetry in a porous medium. Dark gray area is compressed material and light gray represents uncompressed material.

### B.1. Spherical shock wave

Let us assume that the shock compression of a porous material with density  $\rho_0$ , decreases the porosity and results in the production of an incompressible material with density  $\rho_1$ . Now consider a point source explosion (or a source with spherical symmetry) in this medium which is infinite in extent. The explosion will initiate an outwardly expanding spherical shock wave (see Fig. B.1). A snapshot of this event contains an outwardly expanding shell of compressed material ( $\rho_1$ ) enveloping the uncompressed material ( $\rho_0$ ) with inner radius  $r_0$  and outer radius  $R$  (see Fig. B.2). Mass conservation requires that:

$$M = \frac{4\pi}{3} R^3 \rho_0 = \frac{4\pi}{3} (R^3 - r_0^3) \rho_1. \quad (\text{B.1})$$

Solving this equation for  $r_0$  yields

$$r_0^3 = R^3 \left( 1 - \frac{\rho_0}{\rho_1} \right) = R^3 k, \quad (\text{B.2})$$

where  $k$  is the compressibility of the material.

Because we assume that the shocked material is incompressible, the divergence of the velocity field,  $v$  must vanish

$$\nabla \cdot v = \frac{1}{r^2} \frac{\partial}{\partial r} (r^2 v) = 0. \quad (\text{B.3})$$

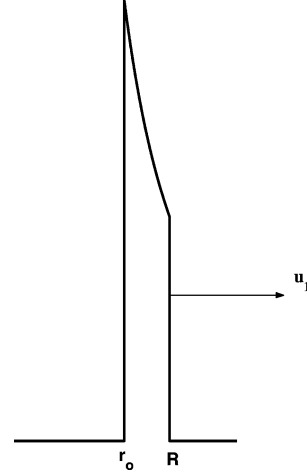


Fig. B.3. Velocity profile of a shock wave with radial symmetry in a porous medium.

Therefore, the velocity profile between  $r_0$  and  $R$  is given by:

$$v(r) = u_1 \left( \frac{R}{r} \right)^2. \quad (\text{B.4})$$

Figure B.3 shows the particle velocity profile that results.

We now recall Eq. (A.1). Solving for  $u_1$  gives

$$u_1 = U_s \left( 1 - \frac{\rho_0}{\rho_1} \right) = U_s k. \quad (\text{B.5})$$

As the shock wave expands into the uncompressed medium, the kinetic energy of the shock wave decreases and is transferred into the newly accreted material. Recall that the amount of kinetic energy gained by the passage of the shock wave is equal to the amount of heat gained by the newly enveloped material (A.3). In the strong shock limit, the strength of the material ( $P_0$ ) can be ignored and the equation of energy loss can be expressed as:

$$-d \left( M \frac{\overline{u^2}}{2} \right) = -\beta d \left( M \frac{u_1^2}{2} \right) \quad (\text{B.6})$$

$$= \frac{u_1^2}{2} dM, \quad (\text{B.7})$$

where  $\overline{u^2}$  is the root mean square velocity in the shocked material and  $\beta$  is the scale factor that relates the two. Before deriving  $\beta$ , let's work out the derivative on the left-hand side of Eq. (B.6). This yields

$$-\beta d \left( M \frac{u_1^2}{2} \right) = \frac{u_1^2}{2} dM,$$

$$-\beta dM \frac{u_1^2}{2} + \beta M u_1 du_1 = \frac{u_1^2}{2} dM.$$

Like terms can be combined and the solution of this differential equation yields the following important relationship:

$$u_1^2 \propto M^{-n}, \quad (\text{B.8})$$

where  $n = (1 + \beta)/\beta$ .

The kinetic energy of the shock wave is given by:

$$E_k = \frac{1}{2} M (\beta u_1^2) \quad (\text{B.9})$$

$$\propto \frac{1}{2} M^{1-n}. \quad (\text{B.10})$$

The kinetic pressure at the interface of the shocked and unshocked aerogel can be found using Eqs. (A.2) and (A.1):

$$P_1 = \rho_0 U_s u_1 = \rho_0 \frac{u_1^2}{k}. \quad (\text{B.11})$$

The kinetic pressure as a function of enveloped mass  $M$  therefore scales as:

$$P \propto M^{-n}. \quad (\text{B.12})$$

This scaling relationship is valid for any kind of shock wave geometry when the energy dissipated in compressing the material is assumed to be negligible. An analytic solution for the general case where  $P_0$  is not ignored can also be found.

The index  $n (= (1 + \beta)/\beta)$  is found by using the velocity profile of the particles in the compressed region, Eq. (B.4). The average particle velocity in the compressed shell ( $r_0 < r < R$ ) is given by:

$$\overline{u_1^2} = \frac{\int_{r_0}^R v^2(r) 4\pi r^2 dr}{\int_{r_0}^R 4\pi r^2 dr}. \quad (\text{B.13})$$

Upon substitution of Eq. (B.4) together with Eq. (B.2), the following relationship emerges:

$$\overline{u_1^2} = \frac{3u_1^2}{(k + k^{2/3} + k^{1/3})}. \quad (\text{B.14})$$

Therefore  $\beta = \frac{3}{(k + k^{2/3} + k^{1/3})}$  for a spherical shock wave. If we take our ideal porous material to be aerogels,  $k \rightarrow 1$ ,  $\beta \rightarrow 1$ , and  $n \rightarrow 2$ .

Equation (B.12) together with the fact that  $M \propto R^3$ , therefore implies that

$$P(R) \propto R^{-6} \quad (\text{B.15})$$

for a spherical shock wave expanding in a perfectly compressible material. For comparison,  $P(R) \propto R^{-3}$  for a shock wave expanding in an incompressible medium. The higher the material porosity, the quicker the shock wave attenuation.

## B.2. Cylindrical shock wave

The derivation of the attenuation properties of a line explosion in a porous medium is similar. Mass conservation in the cylindrical case requires that:

$$M = \pi R^2 \rho_0 = \pi (R^2 - r_0^2) \rho_1. \quad (\text{B.16})$$

Solving this equation for  $r_0$ , we get

$$r_0^2 = R^2 \left( 1 - \frac{\rho_0}{\rho_1} \right) = R^2 k. \quad (\text{B.17})$$

The shocked material is again assumed to be incompressible. The velocity profile between  $r_0$  and  $R$  is now given by

$$v(r) = u_1 \left( \frac{R}{r} \right). \quad (\text{B.18})$$

In addition,  $u_1 = U_s (1 - \rho_0/\rho_1) = U_s k$  as before.

Recalling that the relationship between the shock kinetic pressure and enveloped mass ( $P \propto M^{-n}$ ) was found independently of the shock wave geometry, we can now focus on the finding the index  $n (= (1 + \beta)/\beta)$  for a shock wave with cylindrical geometry. The average particle velocity in the compressed cylindrical shell ( $r_0 < r < R$ ) is now given by:

$$\overline{u_1^2} = \frac{\int_{r_0}^R v^2(r) 2\pi r dr}{\int_{r_0}^R 2\pi r dr}. \quad (\text{B.19})$$

Upon substitution of Eq. (B.18) together with Eq. (B.17) the following relationship emerges:

$$\overline{u_1^2} = \frac{\ln k}{(k-1)} u_1^2. \quad (\text{B.20})$$

Therefore  $\beta = \frac{\ln k}{(k-1)}$  in cylindrical coordinates. In the limit where  $k \rightarrow 1$ ,  $\beta \rightarrow 1$ , and  $n \rightarrow 2$  just as in the spherical case.

For a cylindrical shock wave propagating in an ideal compressible solid, the shock wave is expected to attenuate as:

$$P \propto R^{-4}. \quad (\text{B.21})$$

## References

- Anderson, W.W., 1998. Physics of interplanetary dust collection with aerogel. NASA STI/Recon Technical Report N 98, 97922+.
- Anderson, W.W., Ahrens, T.J., 1994. Physics of interplanetary dust capture via impact into organic polymer foams. *J. Geophys. Res.* 99, 2063–2071.
- Barrett, R.A., Zolensky, M.E., Horz, F., Lindstrom, D.J., Gibson, E.K., 1992. Suitability of silica aerogel as a capture medium for interplanetary dust. In: *Proc. Lunar Planet. Sci. Conf.*, pp. 203–212.
- Brownlee, D.E., Tsou, P., Burnett, D., Clark, B., Hanner, M.S., Horz, F., Kissel, J., McDonnell, J.A.M., Newburn, R.L., Sandford, S., Sekanina, Z., Tuzzolino, A.J., Zolensky, M., 1997. The STARDUST mission: returning comet samples to Earth. *Meteorit. Planet. Sci.* 32, A22 32, 22+.
- Burchell, M.J., Creighton, J.A., Cole, M.J., Mann, J., Kearsley, A.T., 2001. Capture of particles in hypervelocity impacts in aerogel. *Meteorit. Planet. Sci.* 36, 209–221.
- Burchell, M.J., Thomson, R., Yano, H., 1999. Capture of hypervelocity particles in aerogel: in ground laboratory and low Earth orbit. *Planet. Space Sci.* 47, 189–204.
- dePater, I., Lissauer, J.J., 2001. *Planetary Science*. Cambridge Univ. Press, New York.
- Domínguez, G., Westphal, A.J., Phillips, M.L.F., Jones, S.M., 2003. A fluorescent aerogel for capture and identification of interplanetary and interstellar dust. *Astrophys. J.* 592, 631–635.
- Gesser, H.D., Goswami, P.C., 1989. Aerogels and related porous materials. *Chem. Rev.* 89, 765–788.
- Hörz, F., Zolensky, M.E., Bernhard, R.P., See, T.H., Warren, J.L., 2000. Impact features and projectile residues in aerogel exposed on Mir. *Icarus* 147, 559–579.
- Housen, K.R., Holsapple, K.A., 2003. Impact cratering on porous asteroids. *Icarus* 163, 102–119.

- Housen, K.R., Holsapple, K.A., Voss, M.E., 1999. Compaction as the origin of the unusual craters on the Asteroid Mathilde. *Nature* 402, 155–157.
- Kadono, T., 1999. Hypervelocity impact into low density material and cometary outburst. *Planet. Space Sci.* 47, 305–318.
- Kitazawa, Y., Fujiwara, A., Kadono, T., Imagawa, K., Okada, Y., Uematsu, K., 1999. Hypervelocity impact experiments on aerogel dust collector. *J. Geophys. Res.* 104, 22035–22052.
- Melosh, H.J., 1989. *Impact Cratering: A Geologic Process*. Oxford Univ. Press, New York.
- Moner-Girona, M., Roig, A., Molins, E., Martínez, E., Esteve, J., 1999. Micromechanical properties of silica aerogels. *Appl. Phys. Lett.* 75, 653–655.
- Trucano, T.G., Grady, D., 1995. Impact shock and penetration fragmentation in porous media. *Int. J. Impact Eng.* 17, 861–872.
- Tsou, P., 1990. Intact capture of hypervelocity projectiles. *Int. J. Impact Eng.* 10, 615–627.
- Zel'dovich, Y.B., Yu, R.P., 1967. *The Physics of Shock Waves and High Temperature Hydrodynamic Phenomena*, vol. 2. Academic Press, New York.